Materials and Design 110 (2016) 821–829

Contents lists available at ScienceDirect

Materials and Design

journal homepage: www.elsevier.com/locate/matdes

Effect of ion implantation on the physical and mechanical properties of Ti-Si-N multifunctional coatings for biomedical applications

A. Shypylenko [a,b,*], A.V. Pshyk [a,b], B. Grześkowiak [a], K. Medjanik [c], B. Peplinska [a], K. Oyoshi [d], A. Pogrebnjak [b], S. Jurga [a,e], E. Coy [a,*]

[a] NanoBioMedical Centre, Adam Mickiewicz University, Umultowska 85, PL 61614 Poznań, Poland
[b] Sumy State University, Rymskogo-Korsakova 2, 40007 Sumy, Ukraine
[c] Lund University, MAX IV Laboratory, Fotongatan 2, 225 92 Lund, Sweden
[d] National Institute for Material Science (NIMS), 3-13 Sakura, 305-0003 Tsukuba, Ibaraki, Japan
[e] Department of Macromolecular Physics, Adam Mickiewicz University, Umultowska 85, 61-614 Poznań, Poland

HIGHLIGHTS

- Ternary coatings of the Ti-Si-N system were deposited by CAVD method.
- Cu ions with energy of 60 keV and dosage of $D = 2 \times 10^{17}$ ions/cm^2 were implanted.
- A Cu concentration of up to 25% at a depth of 25 nm (maximum implantation depth of 60 nm) was achieved.
- Mechanical properties of the coating have been negatively affected by ion implantation.
- The low dosage of Cu ions did not show any antibacterial activity on the samples, while a rapid release of Cu was observed.

GRAPHICAL ABSTRACT

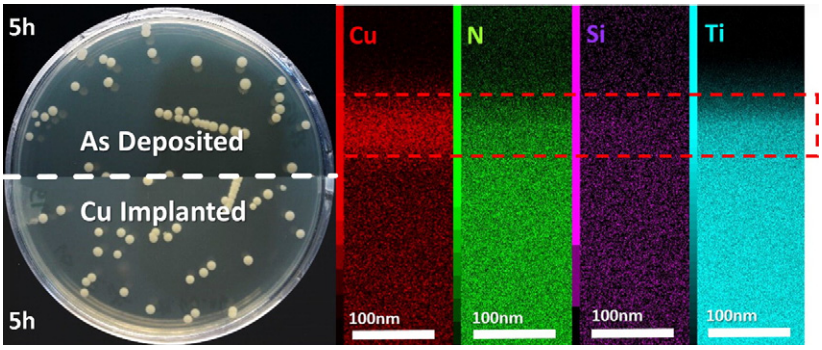

ARTICLE INFO

Article history:
Received 17 June 2016
Received in revised form 28 July 2016
Accepted 15 August 2016
Available online 20 August 2016

Keywords:
TiSiN
Coatings
Antibacterial
Ion implantation
NEXAFS
CAVD

ABSTRACT

In the present work, multifunctional Ti-Si-N coatings have been deposited using CAVD method with the aim of studying their chemical, physical, structural and mechanical properties. Coatings of Ti-Si-N were modified by high-intensity ion implantation using copper ions with dose $D = 2 \times 10^{17}$ ions/cm^2 and energy E = 60 keV. The results demonstrated that ion implantation has an effect on the grain size, hardness, and Young modulus of the Ti-Si-N coating. Additionally, the effect of Cu implantation on the bioactive properties of coatings was investigated by contact antimicrobial essay. The results show a high release of Cu ions in the cultivation liquid and the low efficiency of the <20% Cu doping towards *E. coli* bacteria. Our results bring understanding to the low dosage ion implantation of multifunctional surfaces towards applications and general drawbacks of ion implantation as bioactive tailoring method.

1. Introduction

Nowadays, one of the priorities in the development of science and technology is the creation and manufacture of novel materials. These efforts are fuelled by the increasing interest and applicability of the nanomaterials. An important area of research in nanomaterials and

* Corresponding authors at: NanoBioMedical Centre, Adam Mickiewicz University, Umultowska 85, PL 61614 Poznań, Poland
E-mail addresses: andshy@amu.edu.pl (A. Shypylenko), coyeme@amu.edu.pl (E. Coy).

http://dx.doi.org/10.1016/j.matdes.2016.08.050
0264-1275/

nanotechnology is the surface engineering, which includes the creation of multi-component (multi-function) nanostructured surfaces. This is the case of protective coatings and more specifically nanocomposite coatings, in which nanocrystalline phases, typically of tens of nanometers [1–8] are embedded in an amorphous matrix.

The uniqueness of the nanostructured coatings resides in the high volume fraction of nanocomposites, their superior strength, resilience to dislocations, the possibility of controlling the ratio of volume fractions of crystalline and amorphous phases, and the possibility of mutual coexistence of metallic and nonmetallic elements [9]. Moreover, the bigger volume fraction of the nanostructured phases in the coatings, allows the careful control of the coating properties by modifying their structure and chemical composition. All of these factors allow the creation of nanostructured coatings with improved physico-chemical and tribological properties, which in practice, translate in high values of hardness ($H > 40$ GPa), Young's modulus, strength, thermal stability, and heat and corrosion resistance [6,10]. It is important to mention that a special feature of these so-called superhard materials, in which materials with the same hardness may exhibit different values of the elastic modulus (E), as well as resistance to elastic strain, to failure (H/E) and resistance to plastic deformation (H^3/E^2) [9].

Current industrial trends widely use coatings based on titanium nitride (TiN) [5–8]. TiN coatings have a broad range of applications such as: dental prosthesis, materials for hip joint and heart valve replacements [11]. This wide applicability is due to the fact that TiN films possess a combination of useful properties such as high hardness, wear/corrosion resistance, as well as biocompatibility, all of which have been exhaustively investigated [12]. TiN and TiO_2 films have been known to possess excellent hemocompatibility [9,13], equally important are the results of SiO_2 and TiO_2 ceramics which have shown to promote the formation of Apatite due to the electronegative surface if TiO in a broad range of pH [14], an important results for implantology. Nevertheless, coatings with a broad range of applications have been studied an proposed in the literature, such as: nitrides (TiN, NbN, ZrN, CrN, AlN, etc.), borides (TiB_2, NbB_2, ZrB_2, among others), and oxides (TiO_2, SiO_2, NbO_2, and ZrO_2) [3,4,7].

For biomedical purposes, a wide range of ceramic materials have been used, such as: TiN, ZrO, TiO_2, SiO_2 and some metal-carbides [15] all of which have shown applicability in implantology [16,17,18]. Unfortunately, the high loads required for many orthopaedic and dental implants restrict the selection of biomaterials [12]. Thus, metals and alloys stand up as a type of materials that meet many of these mechanical requirements. [19,20]. Nevertheless, the control of chemical composition of such functional coatings, i.e.: by adding a third component such as (Si), may enable them to significantly improve their mechanical properties and therefore extend their applicability [3,5]. A great interest to the Ti-Si-N coatings resides on their high hardness (≥40 GPa), thermal stability (1100 °C), resistance to oxidation at high temperatures (600 °C) and high resistance to abrasion [13,21,22].

A common approach used to improve the tribological properties of TiN coatings is to apply a high-dose ion implantation [23]. The literature provides sufficient evidence to support the statement that the ion implantation of several atoms N, W, Ni, Mo and Al, can lead to the improvement of the tribological properties of protective coatings [24]. Investigation of the N ion implantation at dose of 1×10^{17}, 5×10^{17} and 1×10^{18} ions/cm^2 on Tungsten metal have revealed that the dose of 1×10^{18} ions/cm^2 could obtain a significant reduction in the friction coefficient of the surfaces [25]. Investigation on the effects of W implantation on the TiN coating shows that increasing implanted materials in the coating can increase hardness and reduce the rate of wear and coefficient of friction [26].

Additionally, ion implantation is one of the most important methods of materials treatment today, and allows the improvement of physical-mechanical properties. Surface properties of materials can be improved without visible changes in the geometry of the samples, furthermore, it introduces different chemical elements into the material, thus changing its surface chemistry. Remarkably enough, it was shown that ion implantation by Cu, Ni or Ti, in the TiN based coatings, can lead to the fabrication of nanocomposites coatings, known for their enhanced mechanical and tribological properties [23]. In addition, it has been also shown that by adding Cu into the nanostructured of nanocomposite coatings their bacteriological properties can be improved [24]. Metal ion implantation in nanostructured or nanocomposite coatings has shown to be a very efficient and promising instrument of controlling and tailoring their physical and functional properties.

Antibacterial tests performed on Cu implanted surfaces have shown that the Cu content strongly influences the antibacterial efficiency of the surfaces, especially in cases when the Cu content reaches values higher than 20 wt.%. Not much consensus is found on the specific reason behind the lack of antibacterial activity on low Cu implanted surfaces, although it is generally attributed to their high roughness and low release rates of Cu^{2+} [27]. Conversely, high Cu ion doping induces higher release of Cu ion from the surface. A high release rate was observed for Ti-Cu alloys with high Cu > 20% content [28], which seems to suggest that low doped surfaces have similar effect, but due to the relatively low Cu ions in the surface, no visible antibacterial activity is reported. Nevertheless, it is quite clear that the Ti-Cu phase should play an important role in a strong antibacterial activity as reported in the literature [29]. Additionally, Cu doping could lead to excellent corrosion resistance and workability of the surfaces, which ultimately has driven important attention of many research groups [29–32].

Although Ti based surfaces are widely applied in the biomedical sector and Cu implantation is commonly acknowledged as an efficient route of tailoring antibacterial surfaces and coatings, there are no studies on the effect of low Cu implantation on Ti-Si-N based coatings, on their physical, mechanical and bioactive properties. This article aims to investigate the effect of low Cu doping on the physical and bioactive properties of Ti-Si-N coatings in order to explore their potential applications in biomedicine.

1.1. Experimental details

Coatings were deposited on A570(36) (steel 3) substrates with polished surface. Substrate dimensions were Ø = 18 mm and t = 3 mm. Coatings were deposited using the cathodic vacuum-arc evaporation (CAVD) technique, operating with Ti and Si cathodes in a nitrogen atmosphere under a high-current. Thickness of the fabricated Ti-Si-N coatings was around 1.2 μm. Deposition parameters are presented in the Table 1. The sample was divided into several pieces in order to investigate the influence of ion implantation on the physical-mechanical properties of the Ti-Si-N coatings. Ion implantation was performed using an ion gun of negative copper ions (Cu^-) [33] with accelerating voltage E = 60 keV, implantation dose was D = 2×10^{17} ion/cm^2.

1.2. Coatings characterization

Elemental composition was investigated using Rutherford Backscattering (RBS) of $4He^+$ ions with energy of 1.7 MeV, detector resolution was E = 13 keV, scattering angle was 170°. Scanning electron microscopy with energy dispersive analysis (SEM with EDX) was also used (JEOL 7001TTLS) in direct and backscattered modes, as well as in elemental

Table 1
Important instrumental parameters in the fabrication of the Ti-Si-N coatings by CAVD.

Parameters	Values
Working pressure N_2 (Pa)	0.3
Ti target current (A)	100
Si targets current (A)	100
Substrate temperature (°C)	>300
Negative bias voltage (V)	−70
Deposition time (min)	220

contrast. Further elemental characterization of the surface was performed by X-ray characterizing irradiation, induced by proton microbeam (μ-PIXE). A scan size of 200 × 200 μm was used on part of the coating's surface, cross-probe size was 4 × 4 μm, charge $Q = 4 \times 10^{-10}$ C/pixel, bitmap 50 × 50 pixels, scanning step 4 μm, energy of protons Ep = 1.5 MeV. Here, a pixel refers to a stationary position of the probe during discrete scan. μ-PIXE spectra were processed using GUPIX software.

Phase composition and structural investigations were done using X-ray diffractometer PANalytical with filtered Cu-Kα radiation (1.5418 Å) with PIXcel 3D detector in Bragg-Brentano geometry. Spectra were recorded in continuous scanning mode at room temperature (300 K), the swept angle was 25.0–80.0 [°2Th.], scanning step was 0.007 [°2Th.] for as-deposited Ti-Si-N samples and 0.0025 [°2Th.] for implanted Ti-Si-N samples. Size of crystallites was evaluated using Scherrer method from the width of the widest band on 37.3372 [°2Th.]. Data were processed in the PANalytical X'Pert software.

Near Edge X-ray Absorption Fine Structure (NEXAFS) experiment has been performed the soft X-ray beamline of the MAX II storage ring at MAX IV lab — Lund University. Accessible energy range is 120 to 2000 eV, with an energy resolving power of around 5000 at the lowest used photon energies. Beamline equipped with a collimated plane grating monochromator and an elliptically polarizing undulator, providing almost 100% linearly and circularly polarized radiation. All measurements were done at room temperature in the so-called "octupole" end station in total electron yield mode (TEY). The advantage of this method is the bulk sensitivity, allowing the investigation of depth information, from 3 to 5 nm depending on studied object and impact angle of the X-ray beam. Two samples (Ti-Si-N after ion implantation by Cu^- ions with $D = 2 \times 10^{17}$ ions/cm^2, E = 60 keV and pure Ti-Si-N) were carefully fixed to the sample holder and loaded into the experimental chamber.

Cross-sections for High Resolution Transmission Electron Microscopy (HR-TEM) were prepared using focused ion beam (FIB) JEOL JIB-4000. Initially a carbon film was applied on top of a rectangular region, in order to protect the sample from the Ga ion beam. Lamellae were then milled down to electron transparency using Ga^+ ion beam with different energy (5–30 keV). HR-TEM measurements were performed on JEOL-ARM 200F (200 kV) equipped with a EDX detector.

Finally, nanohardness and elastic modulus were measured using nanoindentation (Hysitron TI 950 TriboIndenter) with Berkovich diamond indenter. Several tests were conducted at different places of the coating using a maximum load of 10,000 μN. We evaluated values of hardness and elasticity modulus from load-unload curves using Oliver-Pharr method [4–6,8–10].

1.3. Antimicrobial activity determination

The antibacterial activity of the samples was tested on the *E. coli* bacteria using dynamic shake flask method. The bacterial cells were cultured in 5 ml of Luria broth in a sterile 15 ml conical tube. The culture was incubated at 37 °C while being shaken at 220 rpm (MaxQ600 Shaker, Thermo Scientific) for 18–20 h. The culture was then washed twice with sterilized saline (0.9% NaCl) solution by centrifugation for 10 min and then the cell pellet was re-suspended in sterilized saline solution. The actual number of cells used for a given experiment was determined by standard serial dilution. Samples with implanted surface and as-deposited surface were tested and compared, samples were shaken with 5 ml of a bacterial suspension containing 2×10^5 CFU/ml. Then, the suspension was taken after 1 h and 5 h of incubation in 37 °C and diluted appropriately. Then 25 μl of the suspension containing 1010 cells was applied to the surface of as-deposited and implanted surfaces for a comparison, experiments were carried out for 1 and 5 h. The suspension was held in contact with the sample by a sterilized glass plate. The ambient temperature was 24 °C. After exposure, the sample and glass plate were washed in 5 ml of the saline solution and a new diluted suspension was formed. Then, 100 μl of this new diluted suspension was transferred and spread on the surface of Petri dish covered with the L-agar. The agar covered with new diluted suspension was cultivated for 24 h in incubator at 37 °C. The grown *E. coli* colonies were clearly visible and were counted.

2. Results and discussion

Structural characterization is shown in Fig. 1 where the XRD patterns of the Ti-Si-N coatings as-deposited (Fig. 1a) and after ion implantation by Cu^- ions with $D = 2 \times 10^{17}$ ions/cm^2, E = 60 keV (Fig. 1b) are presented. It was found that all the Ti-Si-N coatings had a polycrystalline structure with strong contribution of crystal planes orientations of TiN (111) and Ti_2N (200).

Experiments show that TiN was stabilized (ICCD: 01-087-0629) and Ti_2N (ICCD: 00-023-1455). However, the values are compatible with the solid solution (Ti, Si)N (ICCD: 04-001-9273) which is congruent with the nominal stoichiometry of the target. We calculated the lattice parameter $a_0 = 4.240$ Å corresponding to fcc (111) and (222) crystal system for TiN, the lattice parameter $a_0 = 4.09$ Å corresponding to bcc (112), (103) and (200) crystal system for Ti_2N. Analysis of the calculated lattice data, in particular TiN lattice parameter after ions implantation, indicates a slight expansion of the lattice in the direction (111) — 0.0153 Å and direction (222) — 0.0045 Å. The broadening of these lines can be attributed to the effect of the ion implantation by increasing

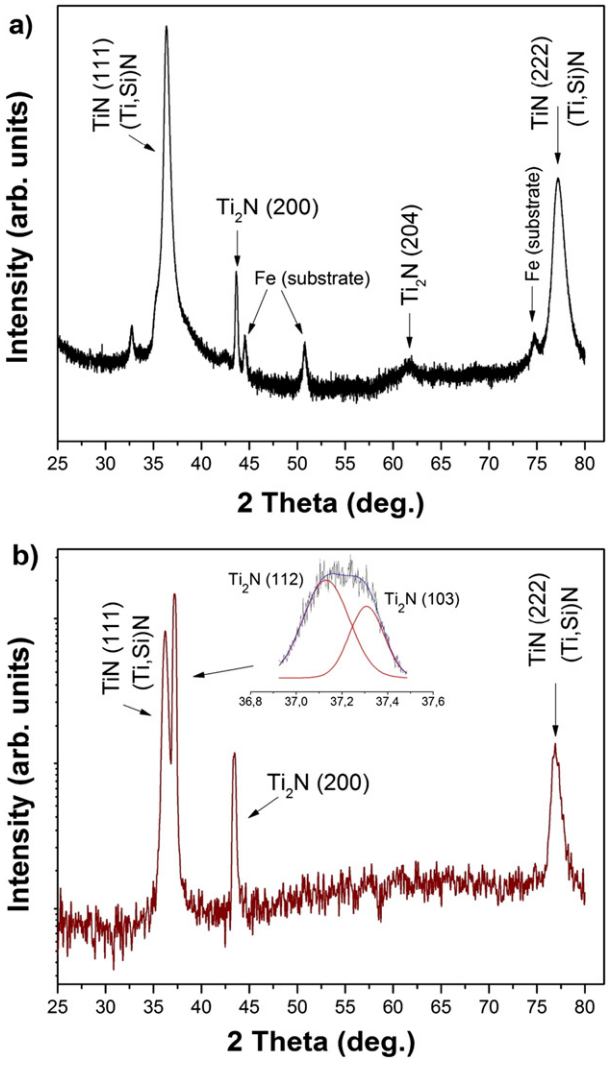

Fig. 1. Ti-Si-N coating's X-ray diffraction patterns: a) as-deposited; b) after ion implantation by Cu^- ions with $D = 2 \times 10^{17}$ ions/cm^2, E = 60 keV.

the misalignment of the grains. Due to similarity of the atomic radii of titanium and copper (Ti = 140 pm, Cu = 135 pm), it can be assumed that the copper ions can create vacancy defect by knocking out titanium atoms from the unit cells, promoting further substitution at both nodes and intermediate positions between lattice sites, thus creating a lattice stresses.

Evaluation of coherent-scattering region (using Scherrer method) showed that the size of nanograins increase from 42.1 nm (as-deposited) to 54.55 nm (after implantation) for TiN, while for as-deposited Ti_2N nanograins this value is reduced from 39.82 nm to 33.56 nm after implantation. Ion implantation is known to induce the decreasing of both transverse and longitudinal sizes of grains [33]. This behaviour is congruent with previous observations, in which high ion implantation lead to a significant decrease of the grain sizes [34]. Nanograins boundaries play an important role in hardening of the material, because they are a barrier for flow spread, as well as dislocations, which form the shear stresses. Therefore, ion implantation, which leads to decreasing of the grain size, might improve the hardness of investigated coatings according to the literature [34,35].

After modelling the XRD pattern of the as-deposited coating using the Rietveld-Toraya model and pseudo-Voigt function [36] in the Powder Cell program [37] and calculating their corresponding volume fraction, a contribution of the cubic phase TiN equal to 66%, and tetragonal phase Ti_2N equal to 34% was found. The analysis of the coating after implantation shows a volume fraction equal to 16.7% (TiN), and 83.3% (Ti_2N). This may indicate that the ion implantation promoted the recrystallization in the coating, which is usually accompanied by a reduction in the strength and hardness of a material and a simultaneous increase in the ductility [4].

Images of the coatings' surface before and after ion implantation by Cu^- 2×10^{17} ions/cm^2 are shown in Fig. 2. As it can be observed, the surface of the coating has a considerable amount of droplets (Fig. 2a,b), which appeared during the deposition of coating by the CAVD. Thus, it is important to remind that a small part of plasma jet in this technique consist of micro droplets. Elemental composition (EDX) of both coatings, as deposited and after ion implantations by Cu^- (D = 2×10^{17} ions/cm^2, E = 60 keV.) is shown in Fig. 2 c and d, the spectra shows an increase of the C and O content, after ion implantation.

From the EDX analysis, the elemental composition of the coating after Cu implantation is extracted as: N = 46.8 at.%, Ti = 35.99 at.%, Cu = 2.19 at.%, Si = 0.30 at.%, O = 3.58 at.% and C = 10.64 at.%. The nominal composition is compatible with that of previously reported samples of Ti-Si-N nanocomposite coatings, N = 54.918 at.%, Ti = 38.78 at.%, Si = 0.418 at.% [37,38]. Additional analysis regarding the elemental composition of the coatings was done using RBS technique (Fig. 3). In the figure, two backscattering spectra are presented: from Ti-Si-N coating as-deposited (Fig. 3a) and after ion implantation (Fig. 3b). According to RBS data, the as-deposited coating mainly consists of Ti, Si and N. The RBS analysis of elemental composition of the Cu implanted (see Fig. 3c) shows that maximal concentration of the Cu ions is around 20 at.% near the surface of the coating. We marked the boundaries of kinematic factors of N, O, Si, Ti and Cu elements. Standard software allowed to receive profiles of elements over the depth of the coating after implantation by Cu^- ions. It can be observed in Fig. 3c, that maximum concentration of implanted ions is observed at a depth of 20–40 nm and that Cu ions reach a maximun depth of ≈60 nm. Oxidized silicon film was also observed at deeper regions, which can be atributed to the ballistic mixing and high density of cascades of collisions between heavy copper ions. Since the Cu implantation was not done in-situ, oxidation of the coating could have started or humidy might have been adsobed on the surface, then, Cu ions pushed their way inside the coating doping the system with surface contaminants. Nevertheless, studies show that Ti, Si and N are the main components of the coating, which are the basis of the (Ti, Si)N solid solution. High concentration of nitrogen was found on the surface of the coating, with a homogeneous distribution over the investigated depth of the coating.

Maps of distribution of elements from the 4 × 4 μm part of the Ti-Si-N coating are presented on the Fig. 4a (as-deposited coating) and Fig. 4b (after ion implantation by Cu^- ions with D = 2×10^{17} ions/cm^2, E = 60 keV), scanning step was 4 μm. Plots clearly show that the distribution of elements is homogeneous on the surface and over the depth studied. Ion implantation led to decrease in Ti concentration and localizing of Si

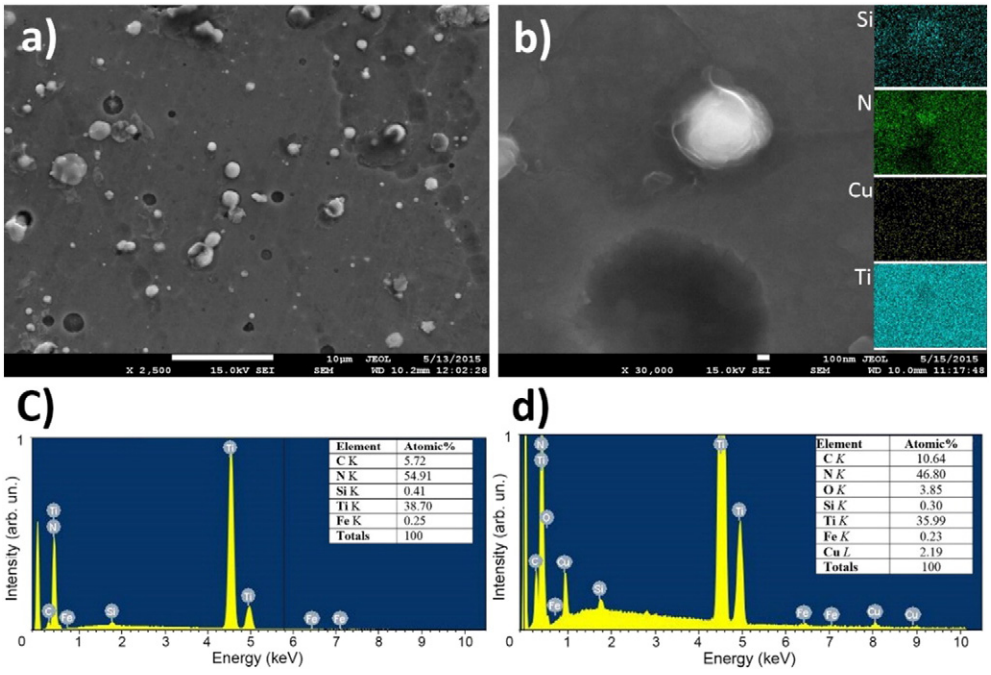

Fig. 2. Surface morphology of the Ti-Si-N coating (a), after ion implantation by Cu^- ions with D = 2×10^{17} ions/cm^2, E = 60 keV. (b) Elemental maps (EDX) of the coatings after ion implantation. EDX spectrograms of as deposited coating (c) and after implantation (d).

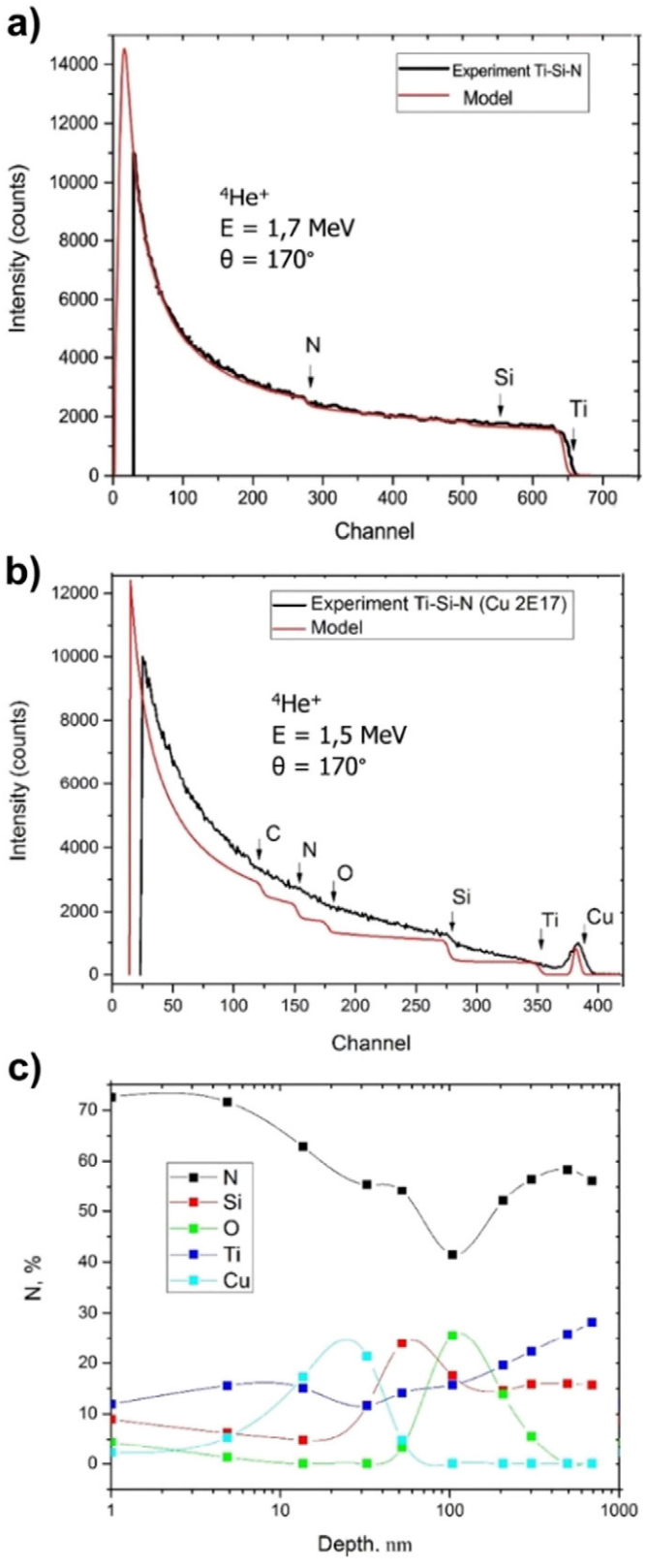

Fig. 3. Energy RBS spectra obtained for coatings: (a) — Ti-Si-N as-deposited, (b) — Ti-Si-N after ion implantation by Cu^- ions with $D = 2 \times 10^{17}$ ions/cm^2, E = 60 keV, (c) — element distribution over depth for the coatings Ti-Si-N after implantation ions Cu^- (2×10^{17} ions/cm^2).

in the regions, which can be easily observed in the Fig. 4b. PIXE-method is not suitable to show such light elements as oxygen and nitrogen, thus we focus on Ti, Cu and Si [38–40].

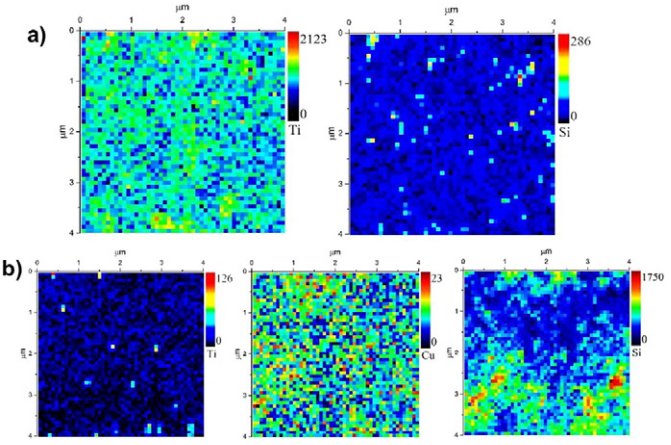

Fig. 4. Element map for a sample fragment with sizes of 2.5 × 2.5 μm (50 × 50 raster and scanning step of 0.5 μm) for the sample of the Ti-Si-N (as-deposited) (a), Ti (left), Si(right)(b) after ion implantation by Cu^- ions with $D = 2 \times 10^{17}$ ions/cm^2, E = 60 keV Ti(left), Cu(centre) and Si(right).

Near Edge X-ray Absorption Fine Structure is presented in Fig. 5. All collected spectra were normalized to the incoming photon beam intensity. Fig. 5a presents NEXAFS spectra where three well defined lines, corresponding to Ti L-edge, Si L-edge and N K-edge of the pure Ti-Si-N, can be observed. Complicated shape of Ti and N signals can be explained by several chemicals interactions in the sample, compatible with the Ti-Si-N, Ti_2N and TiN crystalline structure observed before. It is important to remember that NEXAFS method can provide superficial information, typically 3–5 nm of the samples. Fig. 5 b shows NEXAFS spectra of Ti L-edge, Cu L-edge and N K-edge of the Ti-Si-N sample after ion implantation by Cu ions. Results suggest the strong oxidation of the sample is reflected in very pronounced shoulders at Ti and Cu L-edges. Furthermore, the weak signal of the N K-edge shows the important contribution of the Cu and Ti atoms on top of the sample. Substantial difference in the Ti L-edges and N K-edge of two samples was observed. This observations suggests, that Ti and N atoms have different chemical interactions due to the Cu implantation, which cause by evaporation of the N atoms and recrystallization of the TiN into Ti_2N as shown in XRD. This results correlate with EDX measurements, where rapid drop of N signal was detected in comparison to pure Ti-Si-N [41].

Transmission electron micrograph, presented in Fig. 6a, shows the crystalline nature of the films and Fig. 6b shows the distribution of the elements in the Cu implanted coating. The coating displays a highly crystalline composition, which is compatible with the results presented in XRD micrographs, with a columnar growth mechanism. The total thickness of the coating was found to be 1.2 μm. The electron diffraction pattern (SAED), presented in Fig. 6a, shows a clear set of spots corresponding to Ti-Si-N (ICCD-PDF: 04-001-9273), and Ti_2N (ICCD-PDF: 01-080-3438), which is compatible with the XRD data. The elemental composition of the coatings was determined by EDX measurements, energy dispersive spectra of the coating was analysed and major components resolved. Peaks from Si, N and Ti can be clearly observed and their values were identified as Ti = 43.9% Si = 0.30% N = 49.5%, showing the rather low doping of the $Ti_{1-x}Si_xN$ unit cells with Si. It is important to remark that the cross section was placed in a Cu grid, thus the sample would show small contributions of Cu and C at any point of measurements. Nonetheless, cross section analysis content shows the clear concentration of Cu ions at depths of 60–70 nm, Fig. 6b, region that was also observed in RBS studies. Composition extracted from the area marked with red dashed lines, shows Ti = 40.67% Si = 0.34% N = 45.22% and Cu = 13.78% while the Cu concentration at any other depths remains close to 7%. Nevertheless the values are congruent with the results of RBS, previously presented in this communication. The low Si presence and the slight changes on the TiN valences and structure, suggest the stabilization of solid solution of (Ti, Si) nitride in the as-

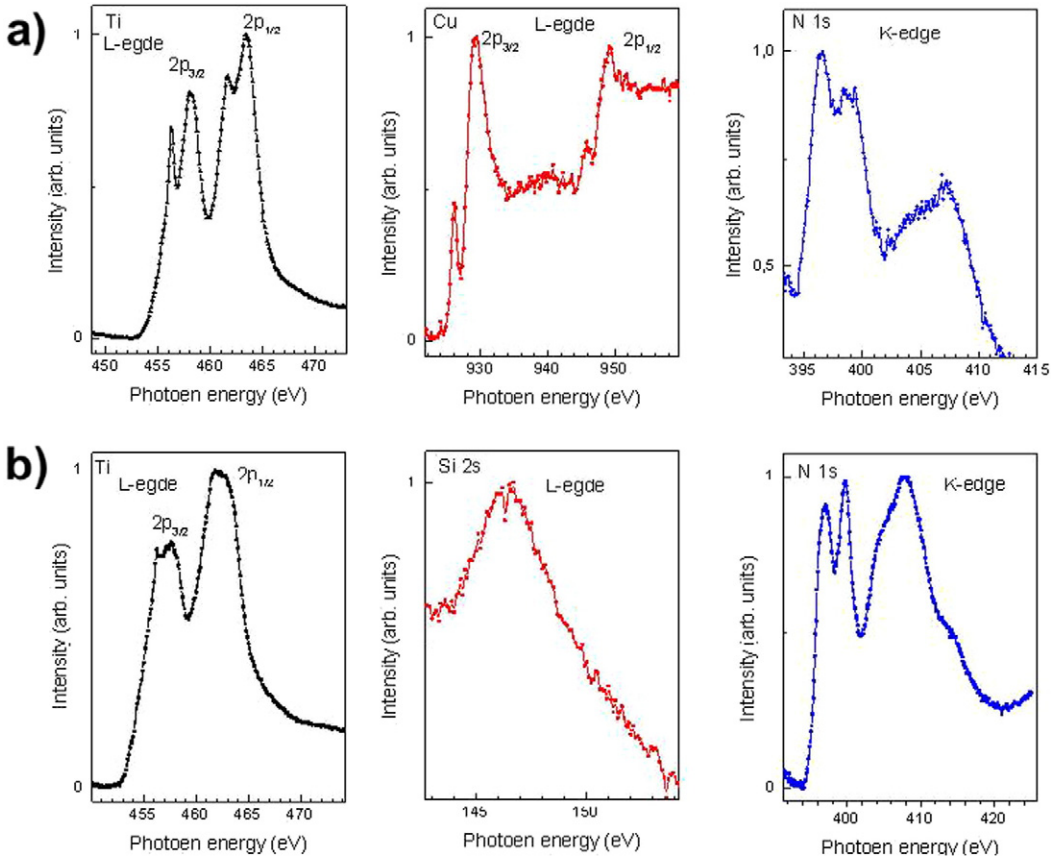

Fig. 5. NEXAFS spectra of pure Ti-Si-N (a) and Ti-Si-N after ion implantation by Cu^- ions with $D = 2 \times 10^{17}$ ions/cm^2 (b), respectively.

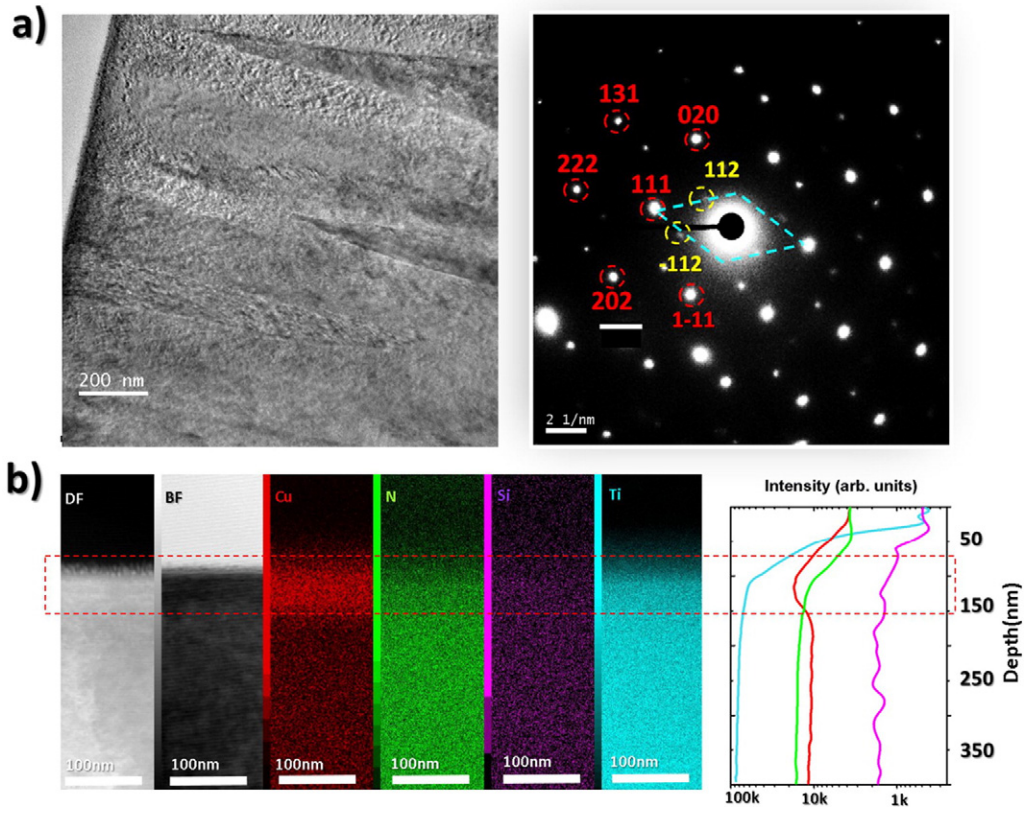

Fig. 6. High resolution micrographs of TiSiN coatings, a) shows the columnar growth of the sample, while the SAED pattern is clearly showing the TiSiN (red dashed circles, zone axis [−101]) and Ti_2N (yellow dashed circles, zone axis [0–11]), b) shows the EDX elemental mapping of the sample with intensity profile of the signals (log scale for clarity).

deposited coating. Moreover, the amount of Si is not sufficient to hinder the grain growth during deposition and for segregation at grain boundaries to form two crystalline phases of the coating. Therefore, columnar structure of the coating is observed. The volume fraction of (Ti, Si)N decreases after ion implantation of Cu ions due to metastable state of (Ti, Si)N with simultaneous increasing of more thermodynamically favourable Ti_2N, which was well demonstrated by XRD. The possible explanation of this phenomenon is a complementary interaction of implantation induced annealing and radiation damage.

Nanoindentation measurements were conducted using a multiple load function applied to a diamond Berkovich tip with maximum loads from 0.05 μN to 10 mN in order to measure hardness (H) and reduced elastic modulus (E_r) at different depths. Nanoindentation experiments for both as-deposited and Cu implanted Ti-Si-N coatings were performed by a partial load/unload function with maximum penetration of 80 nm, well above the maximum Cu concentration of the implanted sample. As it can be observed in Fig. 7, the extracted values of hardness and elastic modulus, based on Oliver-Pharr method, show an average hardness of 23.52 GPa and reduced elastic modulus of 320 GPa for the as-deposited sample. Ion implantation of Cu ions with $D = 2 \times 10^{17}$ ions/cm^2, E = 60 keV leads to slight decrease of reduced elastic modulus to value 290 GPa at the depth 30 nm, increasing to the value ~320 GPa at depth corresponding with the highest Cu concentration. The average hardness value has the same tendency being ~20.36 GPa at the depth up to 30 nm with further increasing up to 22 GPa at the depth 45–65 nm.

Elastic strain prior to plastic deformation (H/E_r) (Fig. 7c) and resistance to plastic deformation H^3/E_r^2 (Fig. 7d) of the coatings had the same tendency as the hardness and reduced elastic modulus (Fig. 7c, d). Nevertheless, the implanted coating has worse elastic strain prior to the plastic deformation after 30 nm, depth at which the hardness values are reliable, which will decrease its wear resistance [3,4,13,21,22]. Moreover, the resistance of the Ti-Si-N coating to the formation of cracks (H^3/E_r^2) decreases after Cu ion implantation, which is well visible in Fig. 7d. The decrease of mechanical properties of the Ti-Si-N coating after Cu ion implantation can be explained by two possible mechanisms. The first possible reason is attributed to the softer Cu-based phase, caused by ion implantation, as shown previously; the surface of the coating has strong contributions of Ti-Cu with rather low Si and N. Another possible explanation is radiation damage, which causes displacements occurring in response to "knock-on" collisions leading to the formation of displacement spikes whose cores may be amorphous. Each such spike will behave as a small second-phase particle in an otherwise damaged matrix and interact with dislocations. The real scenario may be a mixture of both mechanism [38,39,42–45].

Finally, antibacterial efficiency of the films was evaluated and presented in Fig. 8. It is generally acknowledged that copper doping with values higher than 20% show detectable antibacterial efficiency, while maximum performance is the highest with concentrations above 65% [46–48]. In the samples studied in this article, the total doping on the surface was estimated as <20%, so it was expected that after the Cu implantation, with a rather low dosage, the bioactivity of the samples was scarce. Antibacterial efficiency tests showed the low bioactivity of the films during the exposure time used, results show similar behaviour as the ones reported by J. Musil et al. [48] for Cr-Cu-O coatings, with almost indistinguishable effect of low Cu doping on the bioactivity of the samples. Elemental analysis of the surfaces after immersion in the cultivation liquid for 5 h shows the following values: C = 14.51%, N =

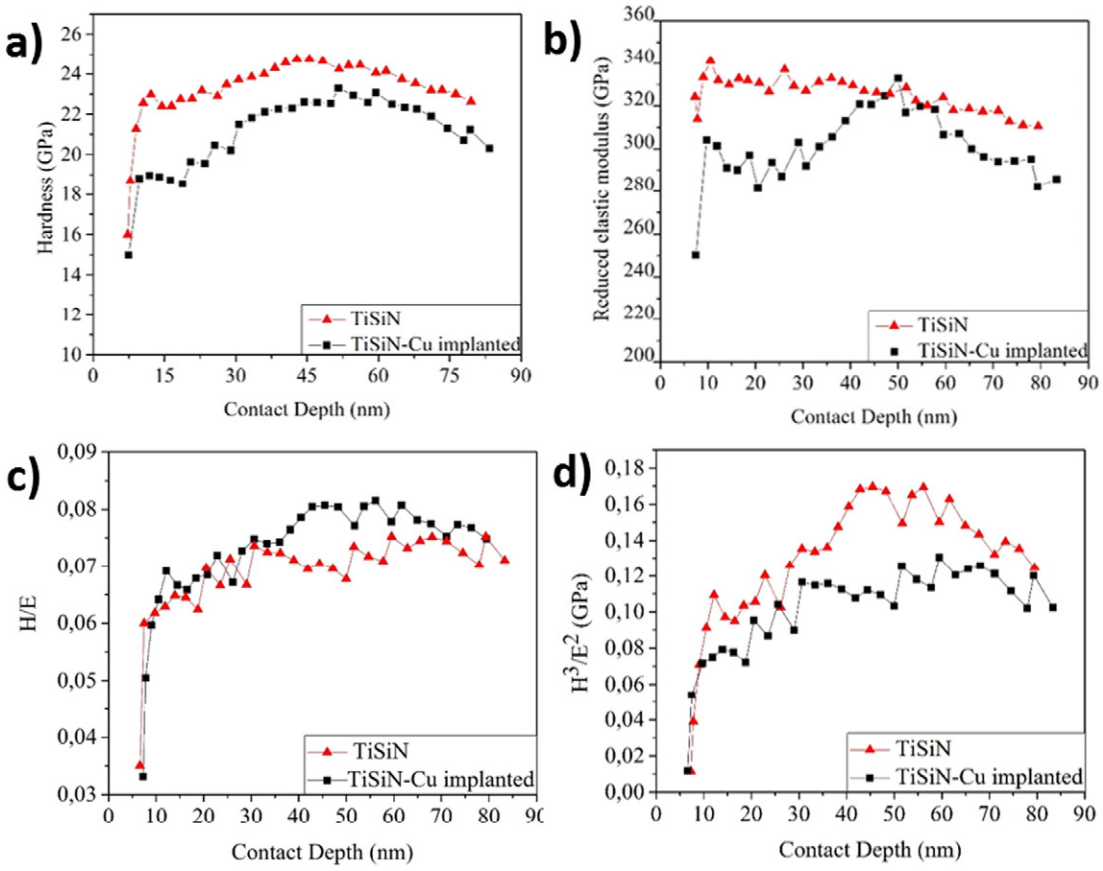

Fig. 7. Hardness (a) and reduced elastic modulus (b) as function of the contact depth and variation of the ratio H/E_r (c) and H^3/E_r^2 (d) as function of contact depth for as-deposited Ti-Si-N coating and after ion implantation of Cu^- ions with $D = 2 \times 10^{17}$ ions/cm^2, E = 60 keV.

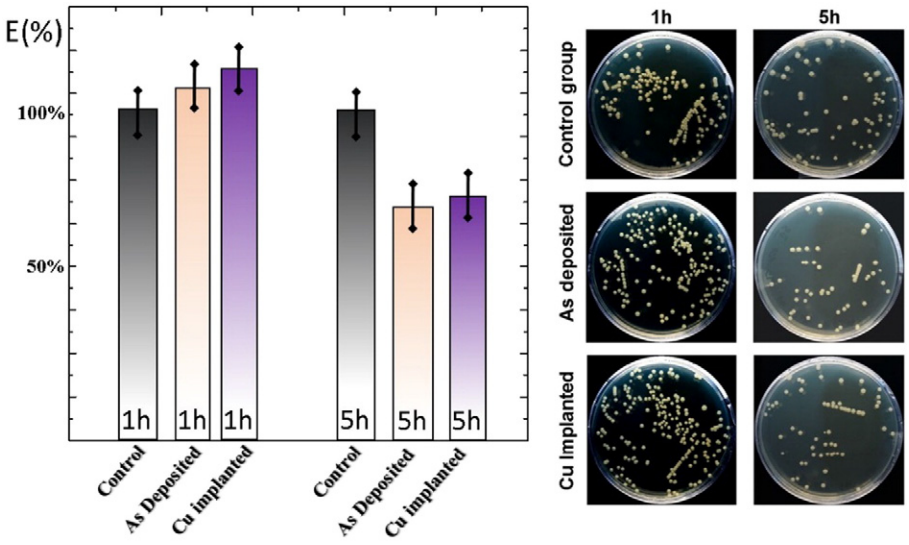

Fig. 8. Antibacterial efficiency E of as-deposited Ti-Si-N and Cu doped surfaces (left) and pictures of the cultivation plates (right).

36.03%, O = 15.28%, Si = 0.5%, Ti = 31.85% and Cu = 1.83%. Results clearly point to a decrease of Cu and N content, while the oxidation of the samples is evident.

Our findings are similar to the ones reported by B. Finke et al. [49] and V. Stranaka et al. [50,51] in which ion implanted Cu surfaces, with doses ranging from 0.7×10^{17} to 63.5×10^{17} ions/cm^2 were used, had lower antibacterial efficiency than surfaces prepared by high pulse magnetron sputtering and the rapid release of Cu was strongly dependent of grain size. This shows the rapid release of Cu ions to the cultivation liquid and is compatible with previous results, in which the first hours of exposure are those in which a bigger Cu release takes place [48].

3. Conclusions

The effect of ion implantation on the physical and mechanical properties of the coatings was studied. The structure of Ti-Si-N coatings on steel was investigated by means of nanoindentation, XRD, SEM (EDS), RBS, μ-PIXE, NEXAFS and TEM. Phase analysis showed that the main crystalline structures, in the as-deposited coating, were (Ti, Si)N, followed by TiN and Ti_2N. Our investigations showed that ion implantation leads to a decrease in grains size and lattice parameter and a worsening of the hardness of the coating (20.36 GPa) and elastic modulus (301 GPa). Bioactivity towards *E. coli* bacteria was studied showing poor antimicrobial effect and rapid Cu release, with 16% of Cu lost under 5 h. The results show the poor stability of the Cu doped surface under the studied conditions and the negative effect on the overall mechanical properties of the films.

Finally, although Cu implantation is a promising and widely studied technique, which has shown an increment of plasticity of the sample, its applicability on bioactive surfaces strongly depends on the ion dosage. The burst effect associated with the rapid release of the Cu ions into the incubation media, although effective for high implantation dosage, could prove inefficient for long lasting functional surfaces and harmful for the environment. Nevertheless, our results serve as a benchmark of the drawbacks of ion implantation on bioactive surface.

Furthers studies are needed in order to understand the burst release effect of these surfaces and generate long lasting bioactive surfaces with fully immobilized Cu ions as antibacterial agent.

Acknowledgments

This work was done with the financial support of the Erasmus Mundus EMINENCE partnership. The authors are grateful to Vladislav Rogoz (Sumy State University) for collaboration regarding the interpretation of XRD and RBS results. We acknowledge MAX-IV Laboratory for providing beam-time. Authors acknowledge the partial financial support from the National Science Centre of Poland by the PRELUDIUM projects number UMO-2015/17/N/ST5/01988 (by EC) and UMO-2015/19/N/ST5/01764 (by A.S & A.P).

References

[1] H. Gleiter, Prog. Mater. Sci. 33 (1989) 233.
[2] R.W. Siegel, Annu. Rev. Mater. Sci. 21 (1991) 559.
[3] S. Veprek, S.A. Reiprich, Thin Solid Films 268 (1995) 64.
[4] A.D. Pogrebnyak, A.P. Shpak, N.A. Azarenkov, V.M. Beresnev, Phys. Usp. 52 (2009) 29.
[5] P.H. Mayrhofer, C. Mitterer, L. Hultman, H. Clemens, Prog. Mater. Sci. 51 (2006) 1032.
[6] J. Musil, Surf. Coat. Technol. 125 (2000) 322.
[7] R.A. Andrievski, Russ. Chem. Rev. 74 (2005) 1061.
[8] J. Musil, Surf. Coat. Technol. 207 (2012) 50.
[9] D.V. Shtanski, S.A. Kulinich, E.A. Levashov, J.J. Moore, Phys. Solid State 45 (2003) 1177.
[10] S. Vepřek, J. Vac. Sci. Technol. A 17 (1999) 2401.
[11] J.J.A.M. Van Raay, P.M. Rozing, C.A. Van Blitterswijk, R.M. Van Haastert, H.K.I. Dion, X. Roques, N. More, L. Labrousse, J. Caix, F. Lefebvre, F. Rouais, J. Gautreau, C. Baquey, Biomaterials 14 (1993) 712.
[12] J.J.A.M. Raay, P.M. Rozing, C.A. Van Blitterswijk, H.K. Koerten, J. Mater. Sci. Mater. Med. 6 (1995) 80.
[13] A.D. Pogrebnjak, A.G. Ponomarev, A.P. Shpak, Y.A. Kunitskii, Phys.-Usp. 55 (2012) 270.
[14] D.V. Shtansky, N.A. Gloushankova, I.A. Bashkova, M.I. Petrzhik, A.N. Sheveiko, F.V. Kiryukhantsev-Korneev, I.V. Reshetov, A.S. Grigoryan, E.A. Levashov, Surf. Coat. Technol. 201 (2006) 4111.
[15] L. Yate, L.E. Coy, D. Gregurec, W. Aperador, S.E. Moya, G. Wang, ACS Appl. Mater. Interfaces 7 (2015) 6351.
[16] S. Mändl, B Rauschenbacha, Surf. Coat. Technol. 156 (2002) 276.
[17] P.A. Dearnley, Proceedings of the Institution of Mechanical Engineers, Part H. (J. Eng. MEd.), 213, Professional Eng. Publ., London, 1999 107.
[18] S. Piscaneca, L.C. Ciacchib, E. Vesselli, G. Comelli, O. Sbaizero, S. Meriani, A. De Vita, Acta Mater. 52 (2004) 1237.
[19] D.V. Shtansky, N.A. Gloushankova, A.N. Sheveiko, M.A. Kharitonova, T.G. Moizhess, E.A. Levashov, F. Rossi, Biomaterials 26 (2005) 2909.
[20] T. Kokubo, H. Kim, M. Kawashita, Biomaterials 24 (2003) 2161.
[21] A. Pogrebnjak, M. Danilionok, V. Uglov, N. Erdybaeva, G. Kirik, S. Dub, V. Rusakov, A. Shypylenko, P. Zukovski, Y. Tuleushev, Vacuum 83 (2009) S235.
[22] A.D. Pogrebnjak, V.V. Uglov, M.V. Il'yashenko, V.M. Beresnev, A.P. Shpak, M.V. Kaverin, N.K. Erdybaeva, Y.A. Kunitskyi, Y.N. Tyurin, O.V. Kolisnichenko, N.A. Makhmudov, A.P. Shypylenko, Ceram. Eng. Sci. Proc. 31 (2010) 127.
[23] A.D. Pogrebnjak, A.M. Tolopa, Nucl. Instrum. Methods Phys. Res., Sect. B 52 (1990) 25.
[24] A. Pogrebnjak, S. Bratushka, N. Levintant-Zayonts, J. Nanoelectron. Phys. 5 (2013) 01016.
[25] R. Martınez, J.A. Garcıa, R.J. Rodrıguez, B. Lerga, C. Labrugere, M. Lahaye, A. Guette, Surf. Coat. Technol. 174-175 (2003) 1253.
[26] B. Tian, W. Yue, Z. Fu, Y. Gu, C. Wang, J. Liu, Vacuum 99 (2014) 68.
[27] J. Fidler, A. Kolitsch, B. Kleffner, G. Henke, S. Stenger, R.E. Brenner, Int. J. Artif. Organs 9 (2011) 882–888.
[28] J. Liu, F. Li, C. Liu, H. Wang, B. Ren, K. Yang, E. Zhang, Mater. Sci. Eng. C 35 (2014) 392.
[29] I.T. Hong, C.H. Koo, Mater. Sci. Eng. A 393 (2005) 213.
[30] J. Banas, A. Mazurkiewicz, Mater. Sci. Eng. A 277 (2000) 183.

[31] L. Nan, K. Yang, J. Mater. Sci. Technol. 26 (2010) 941.
[32] G. Jin, H. Qin, H. Cao, S. Qian, Y. Zhao, X. Peng, X. Zhang, X. Liu, P.K. Chu, Biomaterials 35 (2014) 7699.
[33] N. Kishimoto, Y. Umeda, C. Takeda, G. Lee, V.T. Gritsyna, Nucl. Inst. Methods Phys. Res. B 148 (1999) 1017.
[34] A.D. Pogrebnjak, S.N. Bratushka, V.M. Beresnev, N. Levintant-Zayonts, Russ. Chem. Rev. 82 (2013) 1135.
[35] A.V. Nikonenko, N.A. Popova, E.L. Nikonenko, M.P. Kalashnikov, A. Kurzina, IOP Conf. Ser.: Mater. Sci. Eng. 112, 2016 012032.
[36] R.A. Young, D.I. Wiles, J. Appl. Crystallogr. 15 (1982) 430.
[37] W. Kraus, G. Nolze, J. Appl. Crystallogr. 29 (1996) 301.
[38] A.D. Pogrebnjak, J. Nanomater. 2013 (2013) 780125.
[39] A.V. Pshyk, L.E. Coy, L. Yate, K. Zaleski, G. Nowaczyk, A.D. Pogrebnjak, S. Jurga, Mater. Des. 94 (2016) 230.
[40] V. Ivashchenko, S. Veprek, A. Pogrebnjak, B. Postolnyi, Sci. Technol. Adv. Mater. 15 (2014) 025007.
[41] A. Kowalik, G. Öhrwall, B.N. Jensen, R. Sankari, E. Wallén, U. Johansson, O. Karis, D. Arvanitis, J. Phys. Conf. Ser. 211 (2010) 012030.
[42] L. Pan, Y. Bai, D. Zhang, J. Wang, Rare Metals 31 (2012) 183.
[43] M.S. Ahmed, M. Paul, Z.-T. Jiang, X. Zhao, W. Rickard, Z.-F. Zhou, L.K.Y. Li, Z. Xie, Corros. Sci. 53 (2011) 3678.
[44] J. Fiedler, A. Kolitsch, B. Kleffner, D. Henke, S. Stenger, R.E. Brenner, Int. J. Artif. Organs 34 (2011) 882.
[45] A.D. Pogrebnjak, G. Abadias, O.V. Bondar, O.V. Sobol, V.M. Beresnev, A.V. Pshyk, A.A. Demianenko, K.O. Belovol, D.A. Kolesnikov, H. Komsta, Acta Phys. Pol. A, 125 (2014) 1284.
[46] D.L. Alontseva, S.N. Bratushka, A.A. Borysenko, A.A. Drobyshevska, I.A. Kulik, N.V. Prokhorenkova, A.V. Pshyk, V.N. Rogoz, Metallofiz. Noveishie Tekhnol. 33 (2011) 721.
[47] N. Fredj, J.S. Kolar, D.M. Prichard, T.D. Burleigh, Corros. Sci. 76 (2013) 415.
[48] J. Musil, J. Blažek, K. Fajfrlík, R. Čerstvý, Š. Prokšová, Appl. Surf. Sci. 276 (2013) 660.
[49] B. Finke, M. Polak, F. Hempel, H. Rebl, C. Zietz, V. Stranak, G. Lukowski, R. Hippler, R. Bader, J.B. Nebe, K.-D. Weltmann, K. Schröder, Adv. Eng. Mater. 14 (2012) B224.
[50] V. Stranaka, H. Wulff, P. Ksirova, C. Zietz, S. Drache, M. Cada, Z. Hubicka, R. Bader, M. Tichy, C.A. Helm, R. Hippler, Thin Solid Films 550 (2014) 389.
[51] V. Stranaka, H. Wulffa, H. Reblb, C. Zietzc, K. Arndtd, R. Bogdanowicza, B. Nebeb, R. Baderc, A. Podbielskid, Z. Hubickae, R. Hipplera, 2011, 31, 1512